

Article

# Optical Torque Exerted on a Charged Sphere by a Polarized Bessel Beam

Ping Li <sup>1</sup>, Lingyu Wan <sup>1,\*</sup> , Huilu Yao <sup>1,\*</sup>, Devki N. Talwar <sup>2</sup> , Liuyan Li <sup>1</sup> and Jiang Jiang <sup>1</sup>

<sup>1</sup> Center on Nanoenergy Research, Laboratory of Optoelectronic Materials & Detection Technology, Guangxi Key Laboratory for the Relativistic Astrophysics, School of Physical Science & Technology, Guangxi University, Nanning 530004, China

<sup>2</sup> Department of Physics, University of North Florida, Jacksonville, FL 32224, USA

\* Correspondence: lyw2017@gxu.edu.cn (L.W.); huiluy@gmail.com (H.Y.)

**Abstract:** In the framework of generalized Lorenz–Mie theory, we report here the results of our comprehensive study for analyzing and computing the optical torque (OT) caused by AGVBB on a charged sphere of arbitrary size. The effects of polarization, order, half-cone angle, the position of particle, and the surface charge are carefully considered. The axial and transverse components or OTs are numerically calculated, and the sign reversal of the axial OTs and vortex-like character of the total transverse OTs are mainly discussed. The results reported here are expected to have significant impact on improving the ability of optical manipulation and rotation.

**Keywords:** optical torque; charged sphere; vector Bessel (vortex) beam; GLMT

## 1. Introduction

An  $l^{\text{th}}$  order axicon-generated vector Bessel (vortex) beam (AGVBB) [1–21] with homogeneous polarization state has a helical phase characterized by  $\exp(il\varphi)$ , where  $\varphi$  is the azimuthal angle. The  $l^{\text{th}}$  order vector of an AGVBB carries two types of angular momentum: (i) a spin angular momentum (SAM) corresponding to the polarization and (ii) an orbital angular momentum (OAM) corresponding to the vortex phase [22–24]. Circularly polarized waves carry SAM quantized as  $\pm \hbar$  per photon, and an OAM, which describes the azimuthal angular dependence of photons, is quantized as  $l\hbar$  per photon. Different  $l$ -values correspond to mutually orthogonal OAM modes, and the total number of OAM modes is unbounded. When an AGVBB interacts with an absorptive particle, the angular momentum is transferred from the beam to the particle, causing an OT. The quantitative assessment of OT generated by a vector vortex beam is of paramount importance for improving the ability of optical manipulation and rotation.

In earlier studies, many researchers have devoted their work to the OTs exerted by AGVBB either on an absorptive Rayleigh dielectric [18,25] sphere, magneto-dielectric [26] sphere, and/or a neutral sphere of arbitrary size. These studies have placed special emphases on the sign reversal of axial OTs and the vortex-like behavior of the total transverse OTs for different polarization types. The existing studies on optical torques by the vector Bessel beams assumed that the particles are un-charged. For many practical situations, however, the particles are charged. For example, particles can be charged due to the frequent collision between two particles or contact with reactor walls. The water droplets formed in ocean sprays is also charged. A graphene-coated particles can be modelled by a charged sphere. These particles have excess surface charge, and these surface charges create a very thin metallic layer. It is important to investigate the OT on the charged particle. It is expected that the surface charge could significantly affect the scattered field and optical torque on the particles.

The purpose of this paper is to numerically compute and analyze the OTs on a charged sphere of an arbitrary size placed in an AGVBB. In the framework of a generalized Lorenz–



**Citation:** Li, P.; Wan, L.; Yao, H.; Talwar, D.N.; Li, L.; Jiang, J. Optical Torque Exerted on a Charged Sphere by a Polarized Bessel Beam. *Symmetry* **2023**, *15*, 128. <https://doi.org/10.3390/sym15010128>

Academic Editors: Christophe Humbert and Renxian Li

Received: 8 November 2022

Revised: 19 December 2022

Accepted: 28 December 2022

Published: 2 January 2023



**Copyright:** © 2023 by the authors. Licensee MDPI, Basel, Switzerland. This article is an open access article distributed under the terms and conditions of the Creative Commons Attribution (CC BY) license (<https://creativecommons.org/licenses/by/4.0/>).

Mie theory (GLMT), we meticulously calculate the axial and transverse OTs, including the results of sign reversal of axial OTs and the vortex-like character of the transverse OTs. The effects of polarization, order  $l$ , half-cone angle  $\alpha_0$ , and surface charge on OTs are carefully analyzed. In Section 2, we outline the theory of the OTs on a charged sphere induced by an AGVBB. In Section 3, the computational results are reported and analyzed on the axial and transverse components of OTs, and the sign reversal of the axial OTs and the vortex-like character of the transverse OTs are mainly discussed. The effect of surface charge is also discussed in Section 3, with the concluding remarks presented in Section 4.

### 2. Optical Torque by an AGVBB on a Charged Sphere

As shown in Figure 1, a spherical particle is placed in a polarized Bessel beam, which is generated using an axicon illuminated by a Gaussian beam. The radius of the particle is  $a$ , and the complex refractive index is  $m_1$ . The particle carries excess surface electric charge, which can be expressed by the equivalent surface conductivity  $\sigma_s$ . The charge amount increases from the 0 (neutral particle) to a saturated charges. The half-cone angle of the beam is  $\alpha_0$ , and the wavelength is  $\lambda$ . The refractive index of the surrounding media is  $m_2$ .

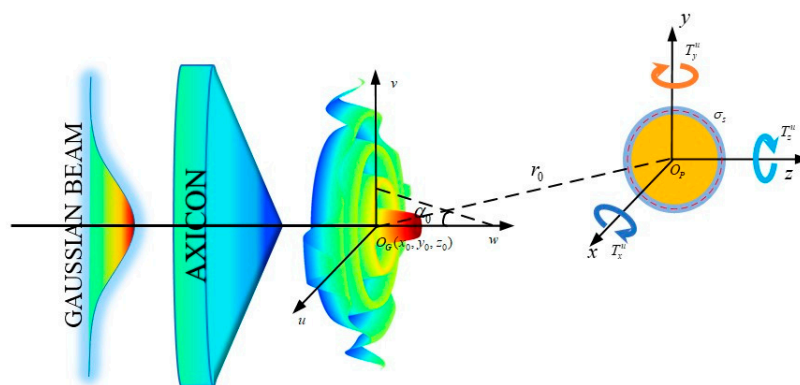


Figure 1. The schematic describing the optical torque exerted on a charged sphere.

Like a neutral sphere, the OT can be expressed by the following [27,28]:

$$\langle T \rangle = - \oint_S \hat{n} \cdot \langle \overset{\leftrightarrow}{A} \rangle \times r dS \tag{1}$$

where  $\langle \rangle$  is a time-average,  $\hat{n}$  is the outward normal unit vector, and  $S$  is a surface enclosing the particle. The Maxwell stress tensor  $\overset{\leftrightarrow}{A}$  is expressed as

$$\overset{\leftrightarrow}{A} = \frac{1}{4\pi} \left( \epsilon \mathbf{E} \otimes \mathbf{E} + \mu \mathbf{H} \otimes \mathbf{H} - \frac{1}{2} (\epsilon E^2 + \mu H^2) \overset{\leftrightarrow}{I} \right) \tag{2}$$

where  $\overset{\leftrightarrow}{I}$  is the unit tensor.  $\mu$  and  $\epsilon$  are the permeability and permittivity of the surrounding media, respectively. The symbol  $\otimes$  denotes a tensor product.  $\mathbf{E}$  and  $\mathbf{H}$  signify the total electromagnetic fields outside the particle and can be derived using GLMT [29]. According to GLMT, the Cartesian components of the OTs are as follows [30–33]:

$$T_x^u = \frac{4m_2}{c} \frac{\pi}{k^3} \sum_{n=1}^{\infty} \sum_{m=1}^n C_n^m \Re(A_n^{m,u}) \tag{3}$$

$$T_y^u = \frac{4m_2}{c} \frac{\pi}{k^3} \sum_{n=1}^{\infty} \sum_{m=1}^n C_n^m \Im(A_n^{m,u}) \tag{4}$$

$$T_z^u = - \frac{4m_2}{c} \frac{\pi}{k^3} \sum_{n=1}^{\infty} \sum_{m=1}^n m C_n^m B_n^{m,u} \tag{5}$$

where

$$C_n^m = \frac{2n+1}{n(n+1)} \frac{(n+|m|)!}{(n-|m|)!} \quad (6)$$

$$A_n^{m,u} = A_n \left( g_{n,TM}^{m-1,u} g_{n,TM}^{m,u*} - g_{n,TM}^{-m,u} g_{n,TM}^{-m+1,u*} \right) + B_n \left( g_{n,TE}^{m-1,u} g_{n,TE}^{m,u*} - g_{n,TE}^{-m,u} g_{n,TE}^{-m+1,u*} \right) \quad (7)$$

$$B_n^{m,u} = A_n \left( |g_{n,TM}^{m,u}|^2 - |g_{n,TM}^{-m,u}|^2 \right) + B_n \left( |g_{n,TE}^{m,u}|^2 - |g_{n,TE}^{-m,u}|^2 \right) \quad (8)$$

$$A_n = \Re(a_n) - |a_n|^2 \quad (9)$$

$$B_n = \Re(b_n) - |b_n|^2 \quad (10)$$

Here,  $\Re$  and the superscript  $*$  denote the real and complex conjugate, respectively.  $K = 2\pi/\lambda$  is the wavenumber. The superscript  $u$  represents the polarization type.  $c$  is the light speed in vacuum.  $a_n$  and  $b_n$  are the Mie scattering coefficients for a charged sphere, which can be written as follows [34–42]:

$$a_n = \frac{\psi_n(x)\psi_n'(m_1x) - m_1\psi_n(m_1x)\psi_n'(x) - i\omega\mu_0\sigma_s/k\psi_n'(m_1x)\psi_n'(x)}{\xi_n(x)\psi_n'(m_1x) - m_1\psi_n(m_1x)\xi_n'(x) - i\omega\mu_0\sigma_s/k\psi_n'(m_1x)\xi_n'(x)} \quad (11)$$

$$b_n = \frac{\psi_n(m_1x)\psi_n'(x) - m_1\psi_n(x)\psi_n'(m_1x) + i\omega\mu_0\sigma_s/k\psi_n(x)\psi_n(m_1x)}{\psi_n(m_1x)\xi_n'(x) - m_1\xi_n(x)\psi_n'(m_1x) + i\omega\mu_0\sigma_s/k\psi_n(m_1x)\xi_n(x)}$$

where  $x = ka$  is the dimensionless size parameter of the sphere.  $\psi_n(\cdot)$  and  $\xi_n(\cdot)$  are Riccati-Bessel functions of first and third kinds, respectively, and the prime indicates the derivative with respect to the parameter. The surface conductivity  $\sigma_s$  is given by the following [34,41,42]:

$$\sigma_s = \frac{i\rho_s e/m_e}{\omega + i\gamma} = \frac{\rho_s e\gamma}{m_e(\omega^2 + \gamma^2)} + i \frac{\rho_s e\omega}{m_e(\omega^2 + \gamma^2)} \quad (12)$$

Here,  $\rho_s$  is the surface charge density, which ranges from 0 to a maximum value. When  $\rho_s = 0$ , the particle is neutral. When  $\rho_s$  has its maximum value, the amount of charge reaches the saturated charges [42].  $e = 1.602 \times 10^{-19}$  C and  $m_e = 9.109 \times 10^{-31}$  kg are the charge and mass of electron, respectively. Following ref. [35], the term  $\gamma$  is defined by  $\gamma \approx k_B T/\hbar$ , with  $T$  being the temperature of the sphere.  $k_B = 1.38 \times 10^{-23}$  J/K is the Boltzmann's constant, and  $\hbar = 1.0546 \times 10^{-34}$  Js is the Planck's constant divided by  $2\pi$ .

$g_{n,TM}^{m,u}$  and  $g_{n,TE}^{m,u}$  are the beam-shaped coefficients (BSCs) [29]. The BSCs for an AGVBB were derived in reference [43,44]. In Equations (3)–(5), a pre-factor involving the power of the incident beam is omitted [33].

### 3. Numerical Results and Discussions

The theory reported in Section 2 is employed here for numerically simulating the vector components of OTs by an  $l^{\text{th}}$ -order AGVBB on the charged sphere having radius  $a$ . Both axial and transverse components of the OTs are discussed separately, with emphasis on the effect of beam order  $l$ , the half-cone angle  $\alpha_0$ , polarization, and the surface charge. Here, we assume that the particle is a pure glycerol droplet surrounded by air of the refractive index  $m_2 = 1$ . The wavelength of an incident beam is  $\lambda = 532$  nm. The real part of the refractive index of the pure glycerol droplet is 1.4746, and the imaginary part is negligible at  $\lambda = 532$  nm [45]. Since the generation of OT needs the absorption of the particle, a small imaginary part of the refractive index is added in our calculation. Thus, the refractive index is assumed to be  $m_1 = 1.4746 + 10^{-7}i$ .

#### 3.1. Axial Optical Torque

We first investigated the axial OT components by placing the charged sphere centered on a zeroth-order ( $l = 0$ ) AGVBB (on-axis,  $x_0 = y_0 = 0$ ), as shown in Figure 1. In our calculations, the surface conductivity is assumed as  $\sigma_s = 5.5 \times 10^{-10} + 4.97 \times 10^{-8}i \Omega^{-1} \text{m}^{-1}$  (corresponding surface charge density is  $\rho_s = 10^{-3}$  C/m<sup>2</sup>). Note that, in this case, the transverse OT components vanish due to the symmetry. Figure 2 describes the calculated

axial OTs ( $T_z^u$ ). The dimensionless size parameter  $ka$  varies in the range  $0 < ka < 10$  with  $k = 2\pi/\lambda$ . The half-cone angle  $\alpha_0$  changes within the range of  $0 \leq \alpha_0 \leq 90^\circ$ . Since the zeroth-order AGVBB with linear, radial, or azimuthal polarization carries neither spin nor the orbital angular momentum, the sphere does not experience axial OT when placed in the beam. In Figure 2, the OTs for these polarizations are not given, and only the OTs for circular polarizations are shown. It can be noted that the axial OTs remain negative (for right circular polarization) and positive (for left circular polarization). This means that the zeroth-order AGVBB for circular polarizations does not reverse the sign of the axial OT. In general, the magnitude of the axial OT is larger for larger size parameter  $ka$  and smaller half-cone angle  $\alpha_0$ .

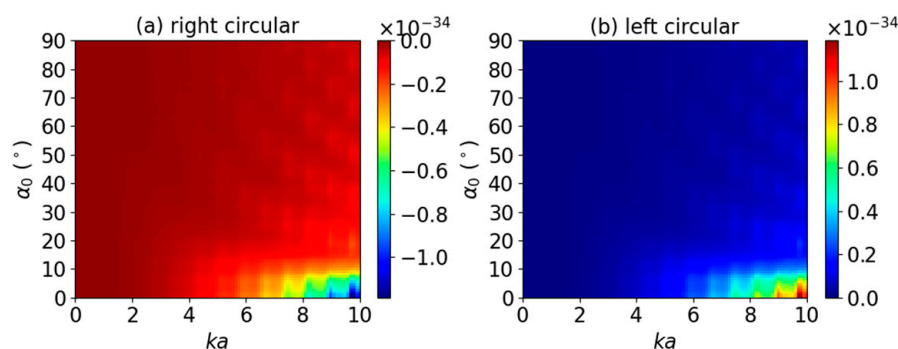


**Figure 2.** The plots for the axial OT  $T_z^u$  of a zeroth-order Bessel beam centered on a charged sphere. The title of each panel denotes the polarization state.

The results displayed in Figure 3 are generated to provide axial OT by the first-order ( $l = 1$ ) AGVBB. It is well-known that a higher-order ( $l \neq 0$ ) AGVBB carries an axial angular momentum denoted by the phase term  $\exp(il\phi)$ . Each photon of the  $l^{\text{th}}$ -order AGVBB carries OAM  $l\hbar$ . In addition, if the incident beam is circular polarized, each photon carries SAM  $+1\hbar$  (left circular polarization) or  $-1\hbar$  (right circular polarization). Thus, the total angular momentum becomes  $(l \pm 1)\hbar$ . When the photons are absorbed or scattered by the particle, the OAM is transferred from incident beam to the particle. Thus, for right circular polarization, the photon carries no angular momentum ( $(l - 1)\hbar = 0$ ), which results in an axial OT of 0 as shown in Figure 3c. Similarly, for left circular polarization, the photon carries angular momentum  $2\hbar$  (Figure 3d), so the magnitude of the axial OT is about twice that of the linear polarizations (Figure 3a,b). The axial OTs for linear polarizations have similar distribution. In general, the magnitude increases with the increase of size parameter  $ka$ . This is caused by the fact that a larger size particle can have more angular momentum from the incident beam, as more rays are incident on the particle. The variation of axial OT with half-cone angle  $\alpha_0$  is dependent on the polarization. For instance, with linear and circular polarization, the maximum axial OT locates in the range between  $40^\circ < \alpha_0 < 70^\circ$ , while that of radial and azimuthal polarizations locates in the range of  $0^\circ < \alpha_0 < 30^\circ$ .

Next, an off-axis case ( $x_0 = 1 \mu\text{m}$ ) is studied for absorptive charged sphere placed in the  $l^{\text{th}}$ -order AGVBB. All other parameters are the same as that of the on-axis case.

Figure 4 depicts the axial OT  $T_z^u$  for a charged sphere illuminated by a zeroth-order ( $l = 0$ ) AGVBB. Similarly, as the AGVBBs for linear, radial, and azimuthal polarizations do not carry any angular momentum, the axial OTs vanish and are not seen in Figure 4. For right (left) circular polarizations, the axial OT remains negative (positive). This means that the sign of the axial OT is not reversed for off-axis incidence. Note that, for a neutral particle, the sign reversal can be observed as discussed in ref. [46]. Thus, depending on the position of particle in the beam, the surface charge can change the sign of the axial OT, namely the rotational direction. The comparison of Figures 2 and 4 shows that the distribution of the axial OTs depends on the position of the particle in the beam.

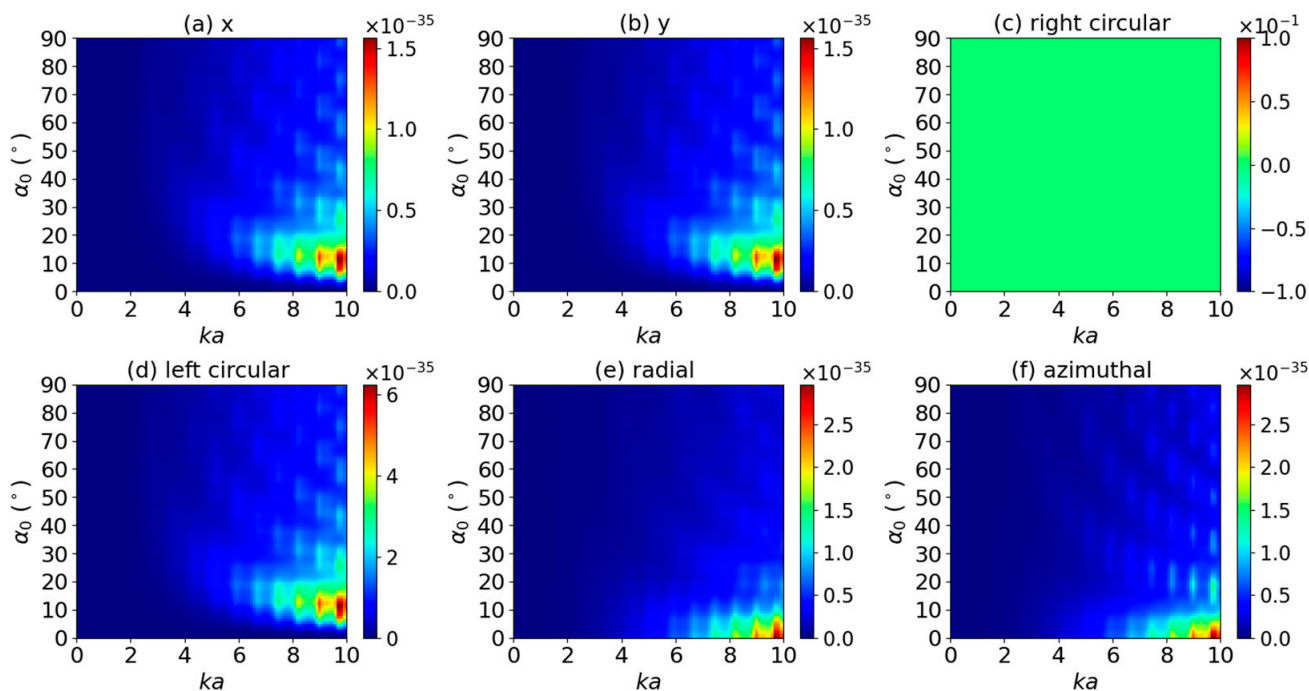


Figure 3. The same as in Figure 2 but with  $l = 1$ .

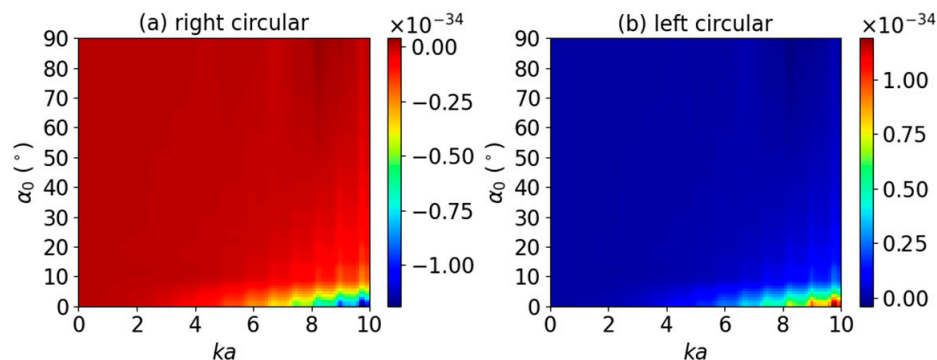


Figure 4. The same as in Figure 2 but with  $x_0 = 1 \mu\text{m}$ .

The effect of increasing the beam order to  $l = 1$  for off-axis incidence is displayed in Figure 5. The comparison of Figures 3 and 5 shows several typical differences of the axial OT  $T_z^u$  for on- and off-axis incidence. The most important difference is that  $T_z^u$  can be either positive or negative depending on the size parameters  $ka$  and half-cone angle  $\alpha_0$ . For instance, if  $ka = 0.8$ , and the beam is linear polarized, the sign of the axial OT changes with  $\alpha_0$ . This means that one can rotate the particle clockwise or counter clockwise by changing the half-cone angle  $\alpha_0$ . This has potential application in the optical switches. Secondly, for right circular polarization,  $T_z^u$  is 0 for on-axis incidence, but it is non-zero for off-axis incidence.

Next, the axial OT  $T_z^u$  is calculated by varying the relative position of the particle and the beam center in the range between  $-1 \mu\text{m} \leq (x_0, y_0) \leq 1 \mu\text{m}$ . Since the surface charge mainly affects small particles, here, we considered relatively small sphere of radius 10 nm. Figure 6 gives the results for a zeroth-order ( $l = 0$ ) AGVBB with half cone-angle  $\alpha_0 = 15^\circ$  and circular polarizations. The OTs for other polarizations vanish and are not shown. For circular polarizations, the axial OTs form a series of concentric rings. In the center, the axial OT has maximum magnitude for left circular polarization, while its magnitude is zero

for right circular polarization. It is seen that the axial OT remains positive (left circular polarization) or negative (right circular polarization), which means that the sign of the axial OT is not reversed.

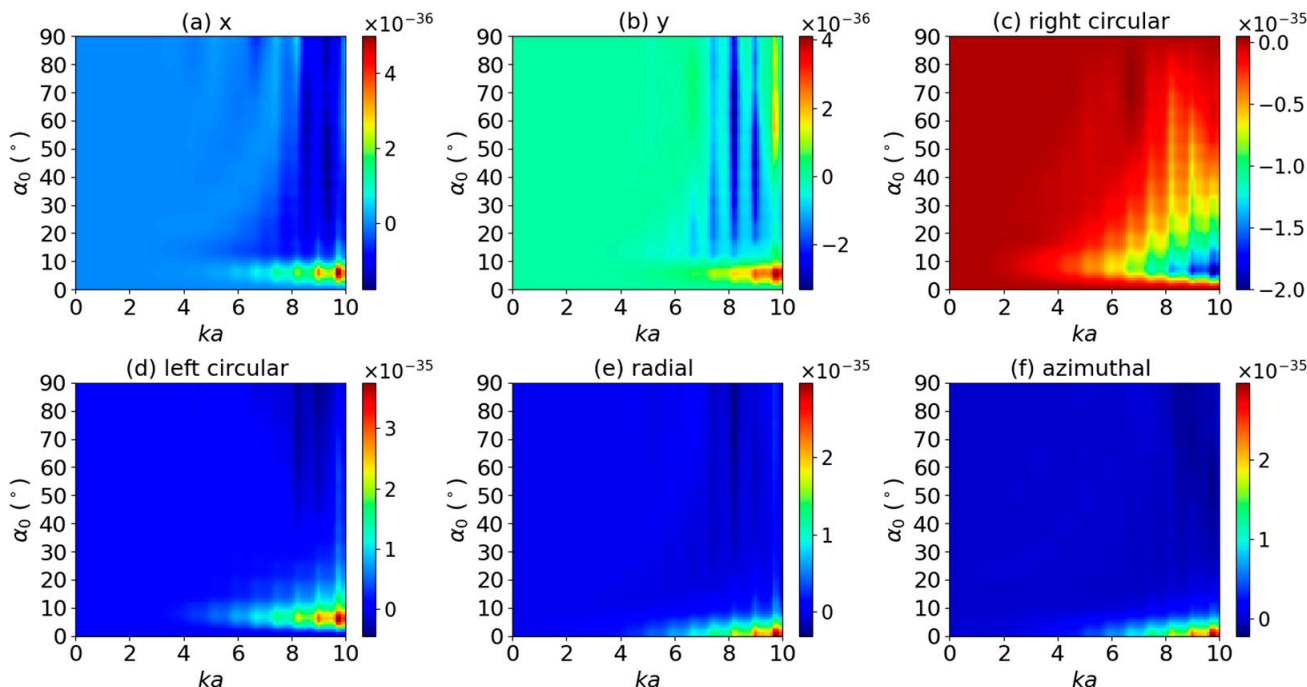


Figure 5. The same as in Figure 4 but with  $l = 1$ .

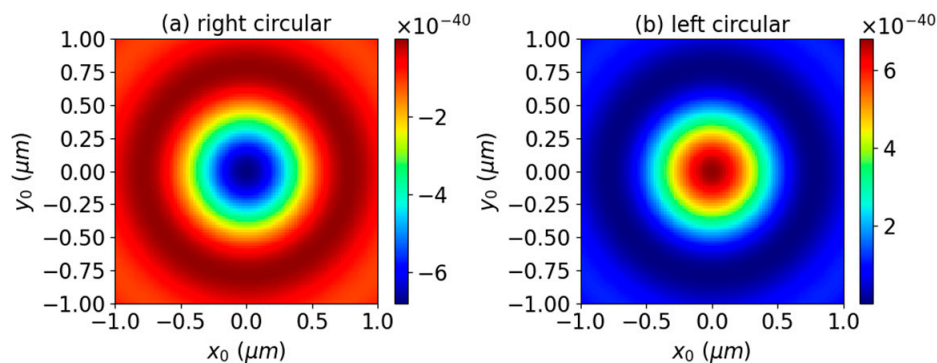


Figure 6. The plots for axial optical torque  $T_z^u$  on a charged sphere in a plane perpendicular to the propagating direction of a zeroth-order Bessel beam.

The effect of increasing the beam order to  $l = 1$  is displayed in Figure 7. First, for circular, radial, and azimuthal polarizations, the axial OTs form a series of concentric rings. For right circular, radial, and azimuthal, the axial OT has central maximum magnitude but zero central magnitude for the left circular polarization. The AGVBBs for radial and azimuthal polarizations induce a larger axial OT than that for the circular polarizations. For circular, radial, and azimuthal polarizations, the axial OTs are symmetrical about the center ( $x_0 = y_0 = 0$ ), while the symmetry is broken for linear polarizations. They form four islands: two of them are formed by maximum magnitude, while the other two are formed by minimum magnitude. For linear polarizations, two islands for minimum magnitude are arranged in the polarization direction, and the other two are perpendicular to the polarization direction. Note that the magnitude for circular polarizations is much larger than that for linear polarizations. It is very important that, for radial and azimuthal polarizations, the axial OT can be positive or negative depending on the position of particle

in the beam. This means that if the particle moves radially from the beam axis, it may rotate in either the counter-clockwise or the clockwise direction.

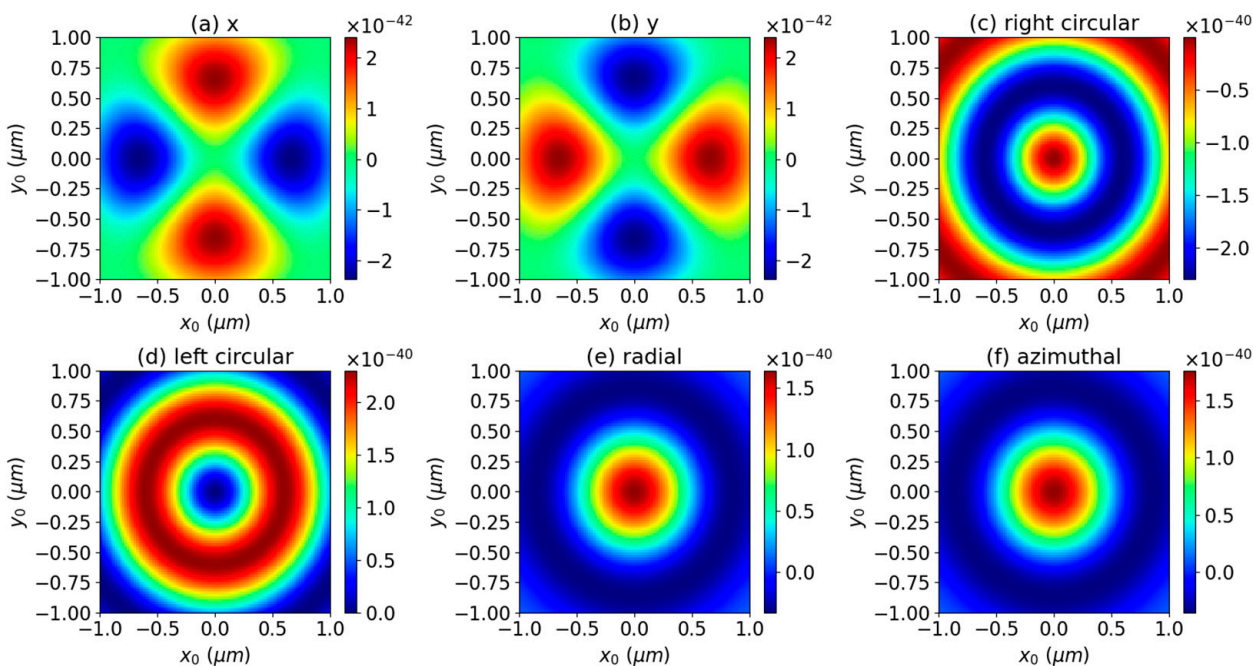


Figure 7. The same as Figure 6 but with  $l = 1$ .

The effects of increasing the half-cone angle to  $\alpha_0 = 80^\circ$  for zeroth- and first-order AGVBBs on the axial OTs were also investigated, and the results are displayed in Figures 8 and 9. Like the smaller half-cone angle, the axial OTs for linear, radial, and azimuthal polarizations are zero, and for circular polarizations, it forms a series of concentric rings. A comparison of Figures 6b and 8b shows an important difference. For left circular polarization, the axial OT for smaller  $\alpha_0$  remains positive, while that of larger  $\alpha_0$  can be either positive or negative depending on the position of the particle. This means that for a larger  $\alpha_0$ , the sign reversal of axial OT can be observed. Similar results can be observed for first-order AGVBB from the comparison of Figures 7d and 9d. Note that for larger  $\alpha_0$ , the concentric rings become denser.

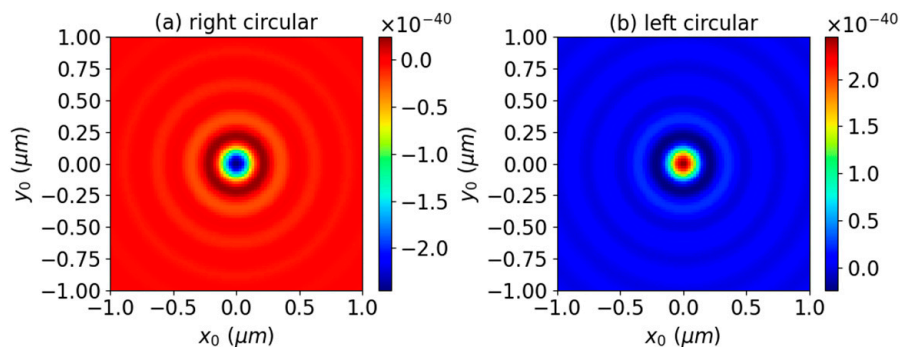
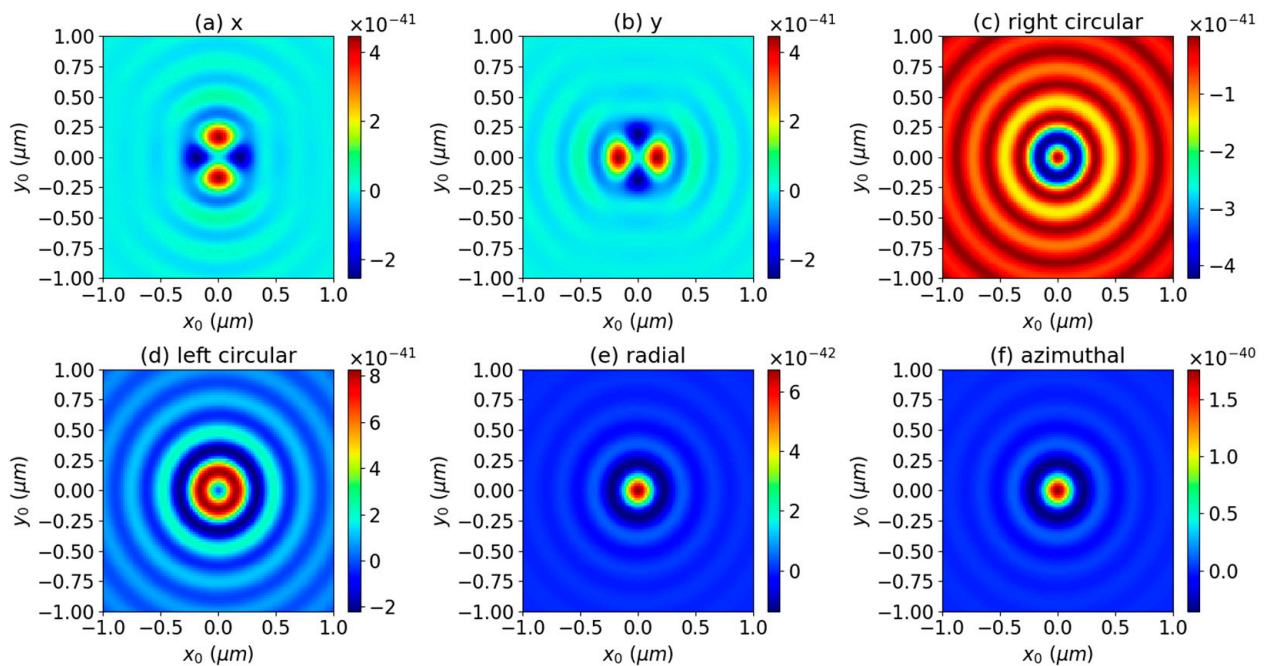


Figure 8. The same as in Figure 6 but with  $\alpha_0 = 80^\circ$ .

### 3.2. Transverse Optical Torque

Next, we investigated the transverse OTs  $T_x^u$  and  $T_y^u$  by considering the effects of polarization, beam order, surface charge, and half-cone angle on the total transverse OT; i.e.,  $T_\perp^u = T_x^u + T_y^u$ . In our calculations, we assumed the radius of the particle  $a = 10$  nm, the refractive index of the particle is  $m_1 = 1.4746 + 1^{-7}i$ , while the surrounding media is air

with refractive index  $m_2 = 1$ . The wavelength of the incident AGVBB is  $\lambda = 532$  nm. The vortex-like character of the transverse OT is mainly discussed.



**Figure 9.** The same as Figure 7 but with  $\alpha_0 = 80^\circ$ .

First, we considered the transverse OTs for a smaller half-cone angle. Figures 10 and 11 show, respectively, the transverse OTs induced by zeroth-order ( $l = 0$ ) and first-order ( $l = 1$ ) AGVBBs with  $\alpha_0 = 15^\circ$ . For the zeroth-order AGVBB with  $x$ -polarization, the transverse OT is parallel or anti-parallel to the  $y$ -axis depending on the position of particle. For  $x_0 > 0$  and  $r_0 = \sqrt{x_0^2 + y_0^2} < 1$ , the transverse OT is parallel to the  $y$ -axis, and it is anti-parallel for  $r_0 > 1$ . For  $x_0 < 0$ , the transverse is opposite to that for  $x_0 > 0$ . The transverse OTs for  $y$  polarization rotate by 90 degrees relative to that for the  $x$  polarization, respectively. For circular, radial, and azimuthal polarizations, the transverse OTs have vortex-like characteristics, and the vortex direction depends on the position of particle. For right circular polarization, the vortex direction is clockwise. For left circular polarization, the vortex direction is counter-clockwise for  $r_0 < 0.7 \mu\text{m}$  and clockwise for  $r_0 > 0.7 \mu\text{m}$ . The transverse OTs for radial and azimuthal polarizations have similar vortex-like character. The vortex direction is clockwise for  $r_0 < 0.9 \mu\text{m}$  and counter-clockwise for  $r_0 > 0.9 \mu\text{m}$ .

Figure 11 shows the transverse OT induced by a first-order AGVBB. Like the zeroth-order AGVBB, the transverse OT generated by a first-order AGVBB with  $x$ -polarization is parallel or anti-parallel to the  $y$ -axis. For  $x_0 > 0$ , the transverse OT is anti-parallel to the  $y$ -axis for  $r_0 < 0.6 \mu\text{m}$  and is parallel to  $y$ -axis for  $r_0 > 0.6 \mu\text{m}$ . For  $x_0 < 0$ , the transverse is opposite to that for  $x_0 > 0$ . Similar to the case of zeroth-order AGVBB, the transverse OTs for  $y$  polarization rotate by  $90^\circ$  relative to that for  $x$  polarization, respectively. Furthermore, vortex-like characteristics can be observed for circular, radial, and azimuthal polarization, but they have different ranges. For right circular polarization, the vortex direction is clockwise for  $r_0 < 0.7 \mu\text{m}$  and anti-clockwise for  $r_0 > 0.7 \mu\text{m}$ . For left circular polarization, the vortex direction is always anti-clockwise. For radial and azimuthal polarizations, the vortex direction is counter-clockwise for  $r_0 < 0.5 \mu\text{m}$ , clockwise for  $0.5 \mu\text{m} < r_0 < 1 \mu\text{m}$ , and counter-clockwise for  $r_0 > 1 \mu\text{m}$ .

In the effect of increasing the half-cone angle to  $\alpha_0 = 80^\circ$ , the transverse OTs is also considered, and the corresponding results for  $l = 0$  and  $l = 1$  are shown in Figures 12 and 13, respectively. For larger  $\alpha_0$ , the transverse OT around the beam axis is much larger than that far away from beam axis, so here, we only discuss the OT in the vicinity of the beam axis.

For linear polarizations, the transverse OT does not have vortex-like character, which is same with that for smaller  $\alpha_0$ . For circular, radial, and azimuthal polarizations, the vortex-like character can be seen near the beam axis for both zeroth- and first-order AGVBBs. The vortex direction for left circular polarization is counter-clockwise, while that for right circular, radial, and azimuthal polarizations is clockwise.

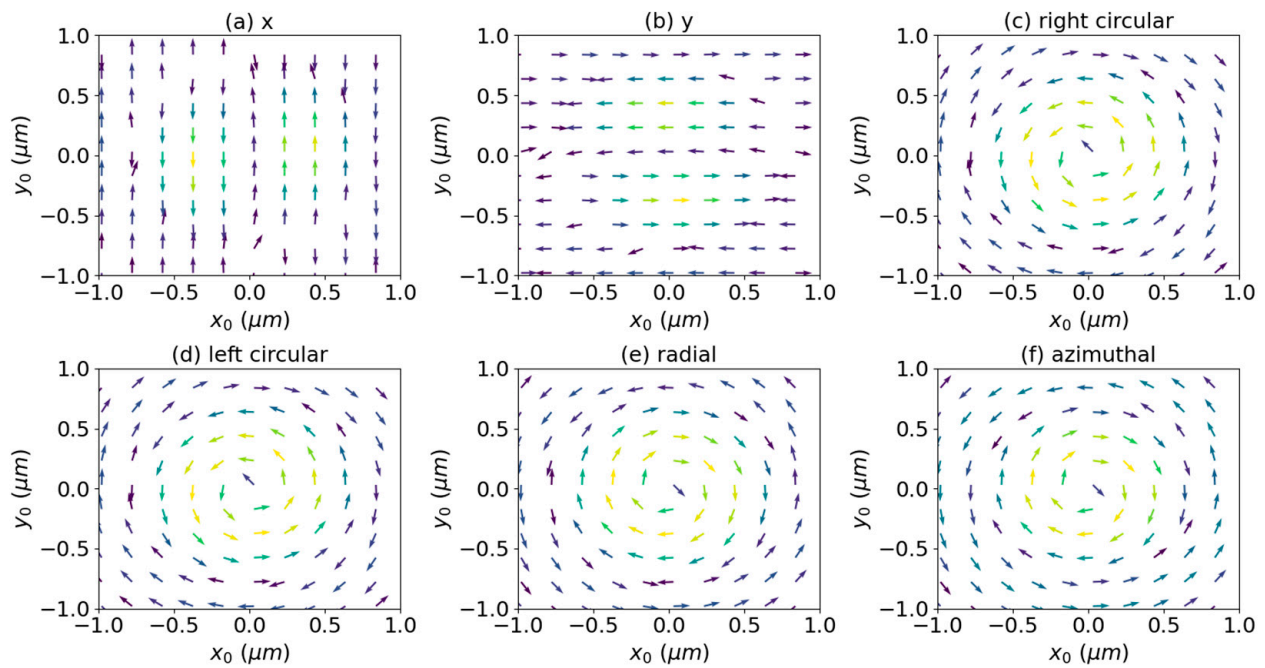


**Figure 10.** Transverse optical torque  $T_{\perp}^z$  produced by a zeroth-order Bessel beam on a charged sphere at  $r = 10$  nm with  $\alpha_0 = 15^\circ$ .

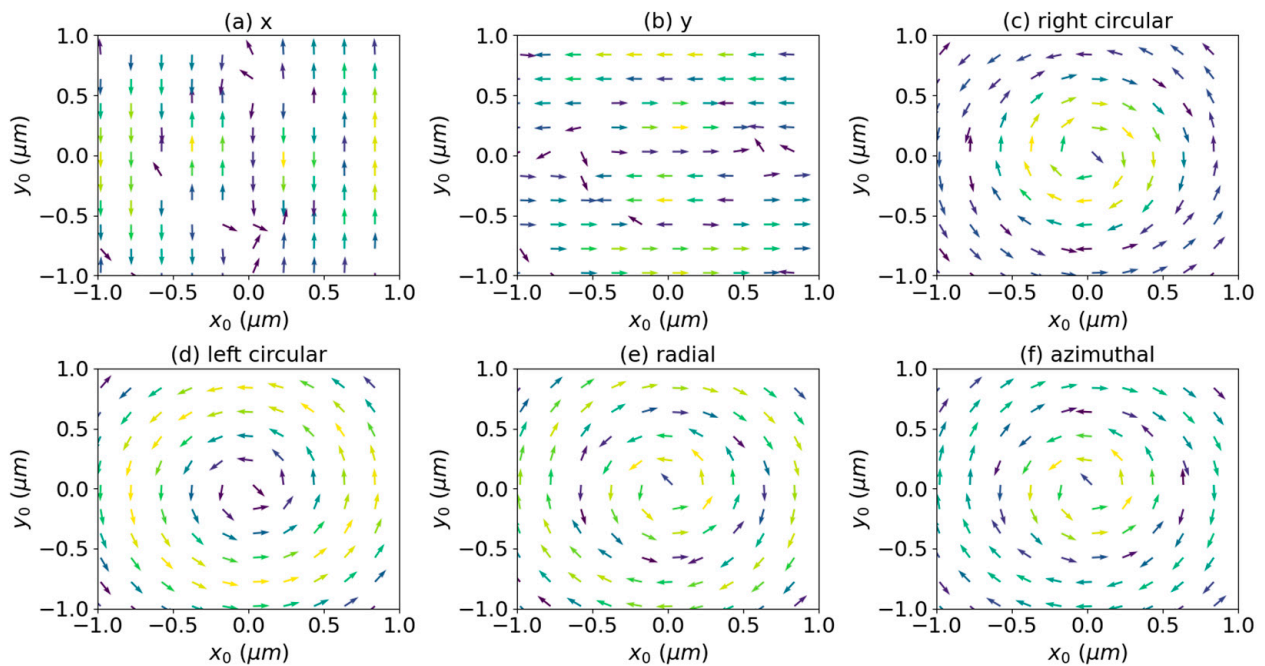


**Figure 11.** The same as in Figure 10 but with  $l = 1$ .

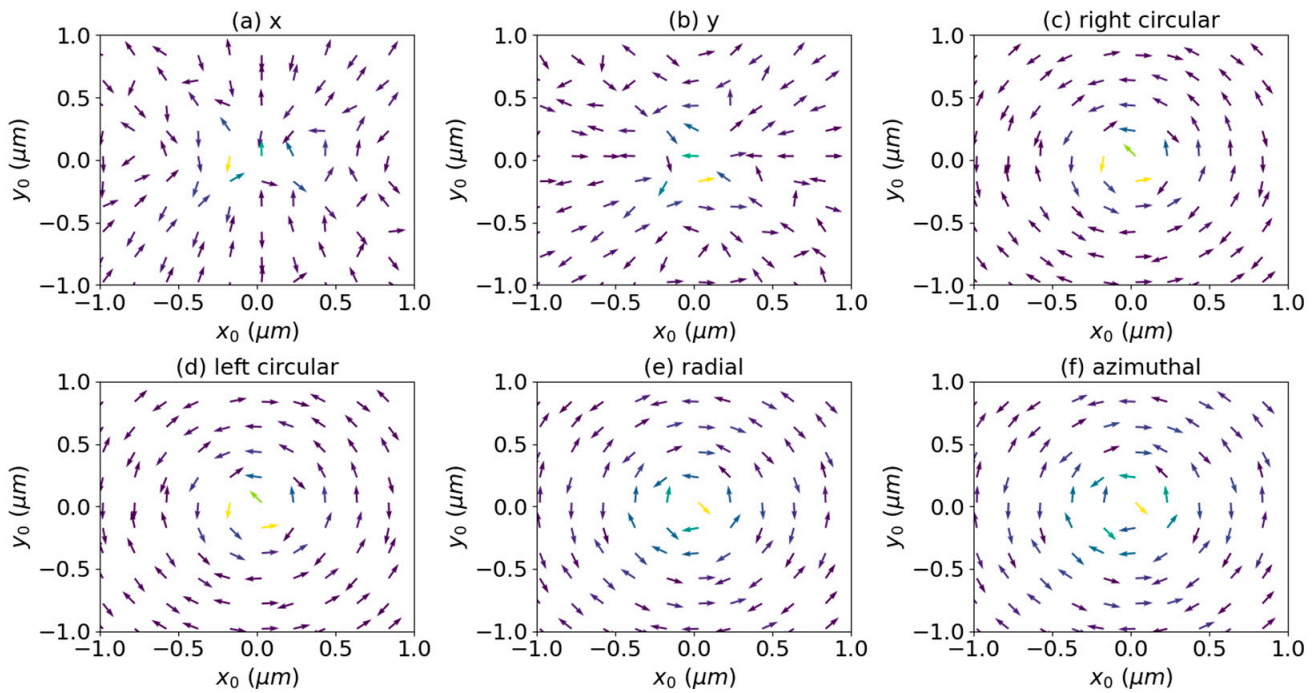


**Figure 12.** The same as in Figure 10 but with  $\alpha_0 = 80^\circ$ .

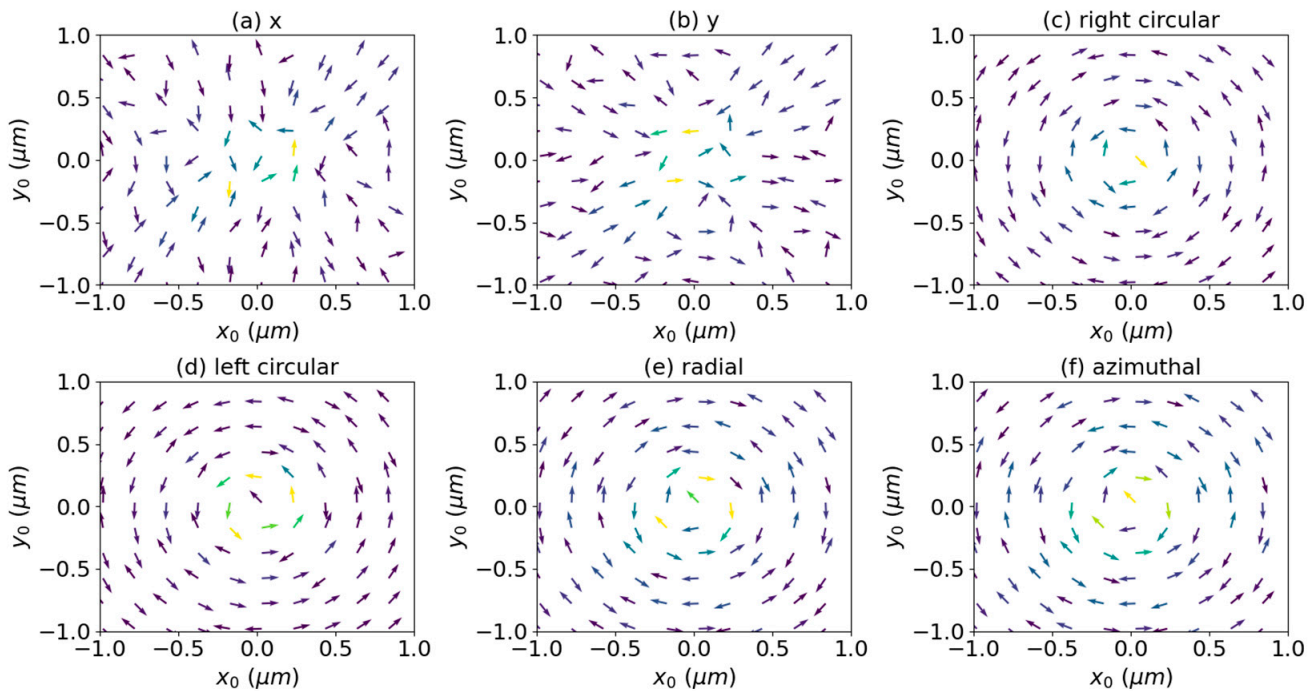


**Figure 13.** The same as in Figure 12 but with  $l = 1$ .

### 3.3. Effect of Surface Charge

In this section, the effect of surface charge on optical torque is mainly discussed. In the calculation, the on-axis ( $x_0 = y_0 = 0$ ) for a charged sphere centered on a Bessel beam is considered. The refractive index of the particle is  $m_1 = 1.4746 + 10^{-7}i$ , and that for the surrounding media is  $m_2 = 1.0$ . The wavelength of the incident beam is  $\lambda = 532$  nm. Here, only the axial OT component  $T_z^u$  are considered.

Figure 14 shows the axial OTs ( $T_z$ ) versus surface conductivity  $\sigma_s$  for particles placed in a zeroth-order ( $l = 0$ ) AGVBB. Various half cone-angle  $\alpha_0$  and size parameters  $ka$  are considered, and  $\sigma_s$  varies from 0 to 1. Note that here, only the results for circular polarizations are given since the OTs for linear, radial, and azimuthal polarizations are zeros. For linear polarizations, the beam carries neither spin nor orbital angular momenta; thus, no angular momenta will be transferred from the beam to the particle, resulting in zero OTs, while for radial and azimuthal polarizations, the axial OTs are zero since the beams have null central intensities. For right circular polarization, the OTs are negative, while the OTs for left circular polarization are positive. This means that the particle does not experience negative axial OTs. With the increasing of  $\sigma_s$ , the magnitude of  $T_z$  increases first and then continuously decreases. For all  $\alpha_0$ , the magnitude of  $T_z$  increases with the size parameter  $ka$ . For right circular polarization, the beam with larger  $\alpha_0$  produces larger OT, while for left circular polarization, larger OT is produced by the beam with smaller  $\alpha_0$ .

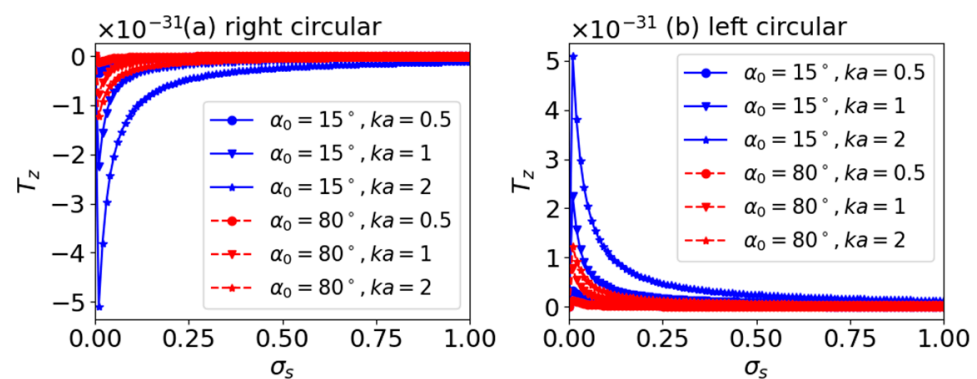


**Figure 14.** The plots for axial optical torque  $T_z^u$  of a charged sphere by a zeroth-order Bessel beam versus  $\sigma_s$ .

The effect of increasing the beam order to  $l = 1$  on the OTs is depicted in Figure 15. Figure 15a–f correspond to linear, circular, radial, and azimuthal polarizations. For right circular polarization, the axial OT is zero. Since each photon of the beam carries both spin angular momentum  $-\hbar$  and orbit angular momentum  $\hbar$ , the total angular momentum carried by the beam is 0, causing the axial OT to vanish. In general, for other polarizations, the axial OTs are all positive. This means that the sphere spins in same handedness of the angular momentum carried by the incident beam. For all cases, the magnitude of the axial OTs increase first and then decreases until to 0. Note that the magnitude for left circular polarization is about twice that for linear polarizations. This is caused by the fact that each photon of a first-order Bessel beam with left circular polarization carries both spin angular momentum  $\hbar$  and orbit angular momentum  $\hbar$ , and the total angular momentum is  $2\hbar$ . For linear and circular polarizations, the OTs change with  $\alpha_0$  and  $ka$  in the same rule. In other words, the magnitude of OTs increases with the increasing of  $\alpha_0$  and  $ka$ , while for radial and azimuthal polarizations, the magnitude decreases with  $\alpha_0$  and increases with  $ka$ .

For quantitatively investigating the effects of the surface charge on axial OT, we calculated the ratio of axial OT  $T_z^u$  for charged and neutral particles. The ratio is defined as  $T_z^c/T_z^n$ , with  $T_z^c$  and  $T_z^n$  denoting the OTs for charged and neutral spheres, respectively.

Figure 16 shows the ratio  $T_z^c/T_z^n$  for a zeroth-order ( $l = 0$ ) AGVBB. Since the axial OT for linear, radial, and azimuthal polarizations is 0, only the OTs for circular polarizations are given in Figure 16. In the calculation, we consider relatively small particles, whose size parameters  $ka$  range from 0.1 to 10. It can be noticed that for both right and left polarizations,  $T_z^c/T_z^n$  decreases with the increase of  $ka$ . This means that the surface charge mainly affects small particles since smaller particles have larger surface charge density.

Once the particle is large enough, the effect can be ignored. In the meanwhile, we can find that the half-cone angle  $\alpha_0$  does not affect the ratio  $T_z^c/T_z^n$ .

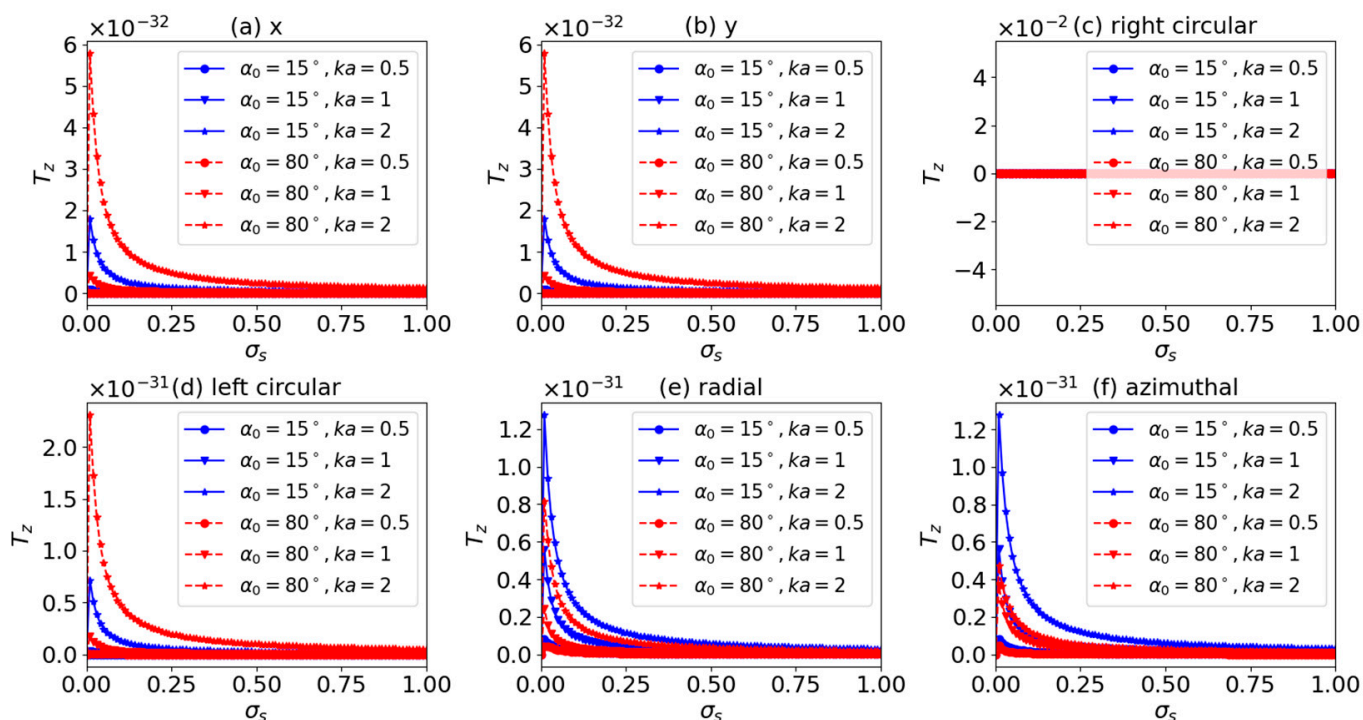


Figure 15. The same as in Figure 14 but with  $l = 1$ .

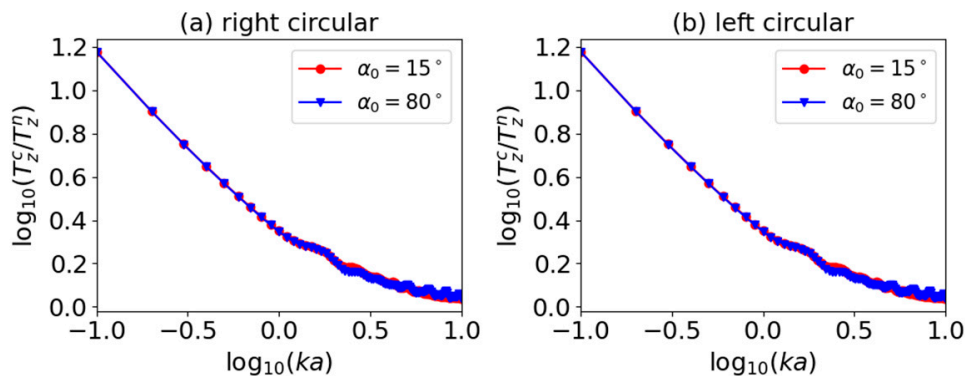


Figure 16. Ratio of axial optical torque for charged and neutral spheres illuminated by a zero-order Bessel beam.

Figure 17 gives the ration  $T_z^c/T_z^n$  for first-order ( $l = 1$ ) AGVBB, where the Figure 17a–f correspond to linear, circular, radial, and azimuthal polarizations. Note that since the axial OT for right circular polarization the axial OT is zero, the corresponding ratio  $T_z^c/T_z^n$  is not given in Figure 17. Similar to the case of zeroth-order ( $l = 0$ ) AGVBB incidence, the ratio  $T_z^c/T_z^n$  decreases with the increase of size parameter  $ka$ . For linear and left circular polarizations, the ratios  $T_z^c/T_z^n$  versus  $ka$  are similar, and the half-cone angle  $\alpha_0$  does not affect the ratio. However, for radial and azimuthal polarizations, the half-cone angle  $\alpha_0$  has influence on the ratio. For instance, if the incident beam is radially polarized, the ratio for a larger angle ( $\alpha_0 = 80^\circ$ ) is larger than that for a smaller angle ( $\alpha_0 = 15^\circ$ ) when the size parameter is small. This means a larger  $\alpha_0$  leads to greater effect of surface charge.

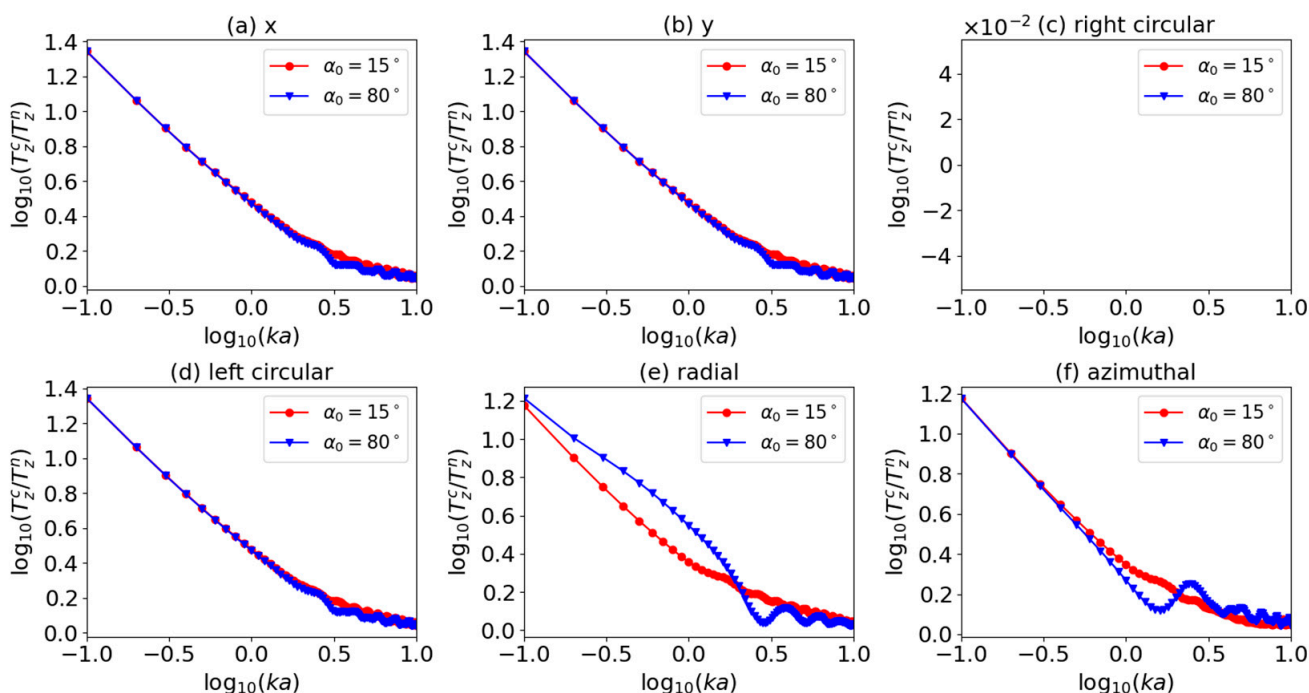


Figure 17. The same as in Figure 16 but with  $l = 1$ .

4. Conclusions

In summary, the OTs on a charged sphere of arbitrary size by an AGVBB were investigated using GLMT. The axial and transverse components of the OTs were separately discussed, and the sign reversal of axial OTs and the vortex-like characteristics of transverse OTs were mainly discussed. To emphasize the effect of surface charge, the axial OT versus surface conductivity  $\sigma_s$  and the ratio  $T_z^c/T_z^n$  versus  $ka$  were calculated. Numerical calculations lead to several conclusions: Like the case of neutral particle, the sign of the axial OT can be reversed, and the vortex-like character of the transverse OT can be observed. The axial OT sign reversal and vortex-like behaviors are highly sensitive to the polarization type, order, and half-cone angle. Secondly, the surface charge does not affect the sign of the axial OT but has strong effect on the magnitude of the axial OT. With the increasing of  $\sigma_s$ , the magnitude of the axial OT increases first and then continuously decreases. Thirdly, with the increase of  $ka$ , the ratio  $T_z^c/T_z^n$  decreases. This means that the surface charge mainly affects the axial OT for a relatively smaller particle. Note that for a neutral particle, the half-cone angle  $\alpha_0$  does not affect the ratio  $T_z^c/T_z^n$ . However, if a charged sphere is illuminated by an AGVBB of radial or azimuthal polarizations, the ratio  $T_z^c/T_z^n$  is sensitive to  $\alpha_0$ . The results reported here are valuable in predicting the OT sign reversal for a absorptive charged sphere of any size in applications dealing with the design and optimization of particle-manipulation devices. Other related applications can also benefit from the results of the present investigation.

**Author Contributions:** Writing—Original Draft, Methodology, Software, and Editing, P.L.; Supervision, L.W.; Validation and Software, H.Y.; Writing—Reviewing, D.N.T.; Data curation, L.L.; Investigation, J.J. All authors have read and agreed to the published version of the manuscript.

**Funding:** This research received no external funding.

**Institutional Review Board Statement:** Not applicable.

**Informed Consent Statement:** Not applicable.

**Data Availability Statement:** Not applicable.

**Conflicts of Interest:** The authors declare no conflict of interest.

## References

1. Mishra, S.R. A vector wave analysis of a bessel beam. *Opt. Commun.* **1991**, *85*, 159–161. [[CrossRef](#)]
2. Bouchal, Z.; Olivik, M. Non-diffractive vector bessel beams. *J. Mod. Opt.* **1995**, *42*, 1555–1566. [[CrossRef](#)]
3. Monk, S.; Arlt, J.; Robertson, D.A.; Courtial, J.; Padgett, M.J. The generation of bessel beams at millimetre-wave frequencies by use of an axicon. *Opt. Commun.* **1999**, *170*, 213–215. [[CrossRef](#)]
4. Arlt, J.; Dholakia, K. Generation of high-order bessel beams by use of an axicon. *Opt. Commun.* **2000**, *177*, 297–301. [[CrossRef](#)]
5. Zhang, Y.; Wang, L.; Zheng, C. Vector propagation of radially polarized gaussian beams diffracted by an axicon. *J. Opt. Soc. Am. A Opt. Image Sci. Vis.* **2005**, *22*, 2542–2546. [[CrossRef](#)]
6. Čizmár, T.; Šiler, M.; Zemánek, P. An optical nanotrap array movable over a milimetre range. *Appl. Phys. B* **2006**, *84*, 197–203. [[CrossRef](#)]
7. Novitsky, A.V.; Novitsky, D.V. Negative propagation of vector bessel beams. *J. Opt. Soc. Am. A Opt. Image Sci. Vis.* **2007**, *24*, 2844–2849. [[CrossRef](#)]
8. Yu, Y.Z.; Dou, W.B. Vector analyses of nondiffracting bessel beams. *Prog. Electromagn. Res. Lett.* **2008**, *5*, 57–71. [[CrossRef](#)]
9. Brzobohatý, O.; Cizmár, T.; Zemánek, P. High quality quasi-bessel beam generated by round-tip axicon. *Opt. Express* **2008**, *16*, 12688–12700. [[CrossRef](#)]
10. Wu, F.T. Geometric optics analysis on self-reconstruction of the nondiffracting beam generated from an axicon. *Acta Phys. Sin.* **2009**, *58*, 3125–3129.
11. Chen, J.; Ng, J.; Wang, P.; Lin, Z. Analytical partial wave expansion of vector bessel beam and its application to optical binding. *Opt. Lett.* **2010**, *35*, 1674–1676. [[CrossRef](#)] [[PubMed](#)]
12. Salem, M.A.; Bağcı, H. Electromagnetic scattering of a vector bessel beam in the presence of an impedance cone. In Proceedings of the IEEE International Symposium on Antennas and Propagation & USNC/URSI National Radio Science Meeting, Orlando, FL, USA, 7–13 July 2013; pp. 1762–1763.
13. Salem, M.A.; Bağcı, H. Behavior of obliquely incident vector bessel beams at planar interfaces. *J. Opt. Soc. Am. A Opt. Image Sci. Vis.* **2013**, *30*, 1172–1179. [[CrossRef](#)] [[PubMed](#)]
14. Li, R.; Guo, L.; Ding, C.; Wu, Z. Scattering of an axicon-generated bessel beam by a sphere. *Opt. Commun.* **2013**, *307*, 25–31. [[CrossRef](#)]
15. Du, T.; Wang, T.; Wu, F. Generation of three-dimensional optical bottle beams via focused non-diffracting bessel beam using an axicon. *Opt. Commun.* **2014**, *317*, 24–28. [[CrossRef](#)]
16. Mitri, F.G.; Li, R.X.; Guo, L.X.; Ding, C.Y. Resonance scattering of a dielectric sphere illuminated by electromagnetic bessel non-diffracting (vortex) beams with arbitrary incidence and selective polarizations. *Ann. Phys.* **2015**, *361*, 120–147. [[CrossRef](#)]
17. Yang, R.; Li, R. Optical force exerted on a rayleigh particle by a vector arbitrary-order bessel beam. *J. Quant. Spectrosc. Radiat. Transf.* **2016**, *178*, 230–243. [[CrossRef](#)]
18. Yang, R.; Li, R.; Qin, S.; Ding, C.; Mitri, F.G. Direction reversal of the optical spin torque on a rayleigh absorptive sphere in vector bessel polarized beams. *J. Opt.* **2017**, *19*, 025602. [[CrossRef](#)]
19. Durnin, J. Exact solutions for nondiffracting beams. i. the scalar theory. *J. Opt. Soc. Am. A Opt. Image Sci. Vis.* **1987**, *4*, 651–654. [[CrossRef](#)]
20. Bouchal, Z.; Wagner, J.; Chlup, M. Self-reconstruction of a distorted nondiffracting beam. *Opt. Commun.* **1998**, *151*, 207–211. [[CrossRef](#)]
21. McGloin, D.; Dholakia, K. Bessel beams: Diffraction in a new light. *Contemp. Phys.* **2005**, *46*, 15–28. [[CrossRef](#)]
22. Volksepulveda, K.; Garceschavez, V.; Chavezcerda, S.; Arlt, J.; Dholakia, K. Orbital angular momentum of a high-order bessel light beam. *J. Opt. B Quantum Semiclass. Opt.* **2002**, *4*, S82–S89. [[CrossRef](#)]
23. Garcés-Chávez, V.; Arlt, J.; Dholakia, K.; Volke-Sepulveda, K.; Chávez-Cerda, S. Orbital angular momentum of a high order bessel light beam. In Proceedings of the Summaries of Papers Presented at the Lasers and Electro-Optics. CLEO '02. Technical Diges, Long Beach, CA, USA, 24 May 2002.
24. Mitri, F.G. Reverse propagation and negative angular momentum density flux of an optical nondiffracting nonparaxial fractional bessel vortex beam of progressive waves. *J. Opt. Soc. Am. A Opt. Image Sci. Vis.* **2016**, *33*, 1661–1667. [[CrossRef](#)] [[PubMed](#)]
25. Mitri, F.G. Negative optical spin torque wrench of a non-diffracting non-paraxial fractional bessel vortex beam. *J. Quant. Spectrosc. Radiat. Transf.* **2016**, *182*, 172–179. [[CrossRef](#)]
26. Li, R.; Yang, R.; Ding, C.; Mitri, F.G. Optical torque on a magneto-dielectric rayleigh absorptive sphere by a vector bessel (vortex) beam. *J. Quant. Spectrosc. Radiat. Transf.* **2017**, *191*, 96–115. [[CrossRef](#)]
27. Stratton, J.A. *Electromagnetic Theory*; McGraw-Hill Book, Co.: New York, NY, USA, 1941.
28. Jackson, J.D. *Classical Electrodynamics*, 3rd ed.; Wiley: New York, NY, USA, 1999.
29. Gouesbet, G.; Maheu, B.; Gréhan, G. Light scattering from a sphere arbitrarily located in a gaussian beam, using a bromwich formulation. *J. Opt. Soc. Am. A Opt. Image Sci. Vis.* **1988**, *5*, 1427–1443. [[CrossRef](#)]
30. Chang, S.; Sang, S.L. Optical torque exerted on a homogeneous sphere levitated in the circularly polarized fundamental-mode laser beam. *J. Opt. Soc. Am. B Opt. Phys.* **1985**, *2*, 1853–1860. [[CrossRef](#)]
31. Barton, J.P.; Alexander, D.R.; Schaub, S.A. Theoretical determination of net radiation force and torque for a spherical particle illuminated by a focused laser beam. *J. Appl. Phys.* **1989**, *66*, 4594–4602. [[CrossRef](#)]

32. Chang, S.; Sang, S.L. Optical torque exerted on a sphere in the evanescent field of a circularly-polarized gaussian laser beam. *Opt. Commun.* **1998**, *151*, 286–296. [[CrossRef](#)]
33. Polaert, H.; Gréhan, G.; Gouesbet, G. Forces and torques exerted on a multilayered spherical particle by a focused gaussian beam. *Opt. Commun.* **1998**, *155*, 169–179. [[CrossRef](#)]
34. Bohren, C.F.; Hunt, A.J. Scattering of electromagnetic waves by a charged sphere. *Can. J. Phys.* **2011**, *55*, 1930–1935. [[CrossRef](#)]
35. Klacka, J.; Kocifaj, M. Scattering of electromagnetic waves by charged spheres and some physical consequences. *J. Quant. Spectrosc. Radiat. Transf.* **2007**, *106*, 170–183. [[CrossRef](#)]
36. Klacka, J.; Kocifaj, M. On the scattering of electromagnetic waves by a charged sphere. *Prog. Electromagn Res.* **2010**, *109*, 17–35. [[CrossRef](#)]
37. Kocifaj, M.; Klacka, J. Scattering of electromagnetic waves by charged spheres: Near-field external intensity distribution. *Opt. Lett.* **2012**, *37*, 265–267. [[CrossRef](#)]
38. Hu, Q.; Xie, L. Scattering phase function of a charged spherical particle. *Appl. Opt.* **2015**, *54*, 8439–8443. [[CrossRef](#)]
39. Xie, L.; Dou, X.Q.; Zhou, J. Sizing charged particles by phase Doppler anemometry. *Appl. Opt.* **2016**, *55*, 3279. [[CrossRef](#)] [[PubMed](#)]
40. Bian, T.; Gao, X.; Yu, S.; Jiang, L.; Lu, J.; Leung, P.T. Scattering of light from graphene-coated nanoparticles of negative refractive index. *Opt. Int. J. Light. Electron Opt.* **2017**, *136*, 215–221. [[CrossRef](#)]
41. Zhou, J.; Dou, X.; Xie, L. Scattering and attenuation of electromagnetic waves by partly charged particles. *J. Quant. Spectrosc. Radiat. Transf.* **2017**, *206*, 55–62. [[CrossRef](#)]
42. Zhou, Z.; Zhang, S.; Qi, J.; Yang, X. Extension of complex refractive index model and analysis of scattering properties of charged submicron spheres. *J. Quant. Spectrosc. Radiat. Transf.* **2020**, *242*, 106735. [[CrossRef](#)]
43. Goodman, J.W. *Introduction to Fourier Optics*; McGraw-Hill: New York, NY, USA, 1968.
44. Mitri, F.G.; Li, R.X.; Guo, L.X.; Ding, C.Y. Optical tractor bessel polarized beams. *J. Quant. Spectrosc. Radiat. Transf.* **2016**, *187*, 97–115. [[CrossRef](#)]
45. Preston, T.C.; Mason, B.J.; Reid, J.P.; Luckhaus, D.; Signorell, R. Size-dependent position of a single aerosol droplet in a Bessel beam trap. *J. Opt.* **2014**, *16*, 025702. [[CrossRef](#)]
46. Li, R.; Ding, C.; Mitri, F.G. Optical spin torque induced by vector bessel (vortex) beams with selective polarizations on a light-absorptive sphere of arbitrary size. *J. Quant. Spectrosc. Radiat. Transf.* **2017**, *196*, 53–68. [[CrossRef](#)]

**Disclaimer/Publisher’s Note:** The statements, opinions and data contained in all publications are solely those of the individual author(s) and contributor(s) and not of MDPI and/or the editor(s). MDPI and/or the editor(s) disclaim responsibility for any injury to people or property resulting from any ideas, methods, instructions or products referred to in the content.